DINAME 2023 - Proceedings of the XIX International Symposium on Dynamic Problems of Mechanics,
A.S. De Paula, A.T. Fabro and M.R. Machado (Editors), ABCM.
Pirenópolis, Go, Brazil, February 26th to March 3rd, 2023

Real-Time capable Multibody Model of dual Truck Front Axles

Georg Rill

OTH Regensburg, Galgenbergstr. 30, 93053 Regensburg, Germany

Abstract: Dual front steering axles are quite common in multi-axled heavy duty trucks. In standard layouts of such axle combinations, the steer motions of the wheels depend not only on the rotation of the steering wheel but also on the movements of the axles. As a consequence, the model complexity of the steering system should match with the complexity of the suspension model. The development of new technologies like advanced driver assistance systems or autonomous driving can only be accomplished efficiently using extensive simulation methods. Such kind of applications demand for computationally efficient vehicle models. This paper presents a steering system model for dual front axles of heavy duty trucks which supplements the suspension model of the axles. The model takes the torsional compliance of the steering column as well as the stiffness of the tie rods and the coupling rod into account. A quasi-static solution provides a straight forward computation including the partial derivatives required for an efficient implicit solver. The steering system model matches perfectly with comparatively lean, but sufficiently accurate multibody suspension models.

Keywords: Steering System, Dual Axles, Multibody Model, Vehicle Dynamics, Real-Time

INTRODUCTION

The multibody system approach to vehicle dynamics has become a standard (Bruni et al., 2020). A multibody approach, which takes the specific features of trucks into account, is illustrated in Rill et al. (2021). Complex models are usually separated into several subsystems including the tires, the steering system, the suspension, and the vehicle frame work (Rill, 2006a). Handling tire models, like TMeasy as described in Rill (2013), provide a useful compromise between accuracy and computation effort. A sophisticated modeling technique combined with an partial implicit solver, tailored to the structure of general vehicle models, makes real-time applications possible even on small computers (Rill 1997). Leaf spring suspended front axles are still very popular in particular at heavy duty trucks. A lumped link model, where in a quasi-static approach the leaf springs act as generalized force elements, suspending and guiding the axle carrier, is described and studied in Rill et al. (2022). Dual front steering axles suspended by leaf springs are quite common in multi-axled heavy duty trucks. The modeling of the suspension and the steering system is quite a challenging task. In particular, if one is interested in lean but sufficient accurate multibody models, which grant low computation costs and make real-time applications possible even on small computers. The works of Qin et al. (2012) and Topaç et al. (2019) apply the commercial software package ADAMS or ADAMS/CAR, respectively, for the analysis and the optimization of the dual axle steering mechanism.

This paper presents a steering system model which fits perfectly to comparatively lean, but sufficiently accurate multibody suspension models. It takes, in a quasi-static approach, the torsional compliance of the steering column as well as the stiffness of the tie rods and the coupling rod into account.

THE MULTIBODY SYSTEM APPROACH TO VEHICLE DYNAMICS

General Layout of Dual Front Axles

The model of a virtual test truck (VTT) presented in Rill et al. (2021) encompasses just one front axle. However, the modular structure makes it possible to supplement the VTT model with a generic subsystem which optionally includes a second front axle and a more complex steering system acting on both axles.

In general, the axle carriers of the two single tired front axles are guided and suspended by leaf springs, Fig. 1. Each axle is composed of the axle carrier, two knuckles and two wheels. The displacements ξ_{Ai}, η_{Ai}, ζ_{Ai}, and the rotation angles α_{Ai}, β_{Ai}, γ_{Ai} describe the momentary position and orientation of the axle carriers $i = 1,2$ relative to the vehicle-fixed frame V. The angles δ_{ij} describe the king pin rotations of the left ($j = 1$) and right ($j = 2$) knuckles relative to the axle carriers $i = 1,2$. Handling tire models like TMeasy (Rill, 2013) consider the tire as a massless force element. Then, each wheel consisting of the rim and the tire forms one rigid body, which performs the rotation φ_{ij} about an axis fixed to the knuckle.

The steering system consists of the steering column, the steering box, the pitman arm, the tie rods 1 and 2, the coupling rod, the coupling lever, and the track rods 1 and 2. The steering box transfers the steer input δ_S to the rotation of the pitman arm. The steering linkage is located here on the left side of the vehicle. As a consequence, the rotation of the pitman arm is transferred via the coupling rod to the coupling lever and via the tie rod 1 to the rotation δ_{11} of the left knuckle relative to the axle carrier 1. The tie rod 2 transmits the rotation of the coupling lever to the rotation δ_{21} of the left knuckle relative

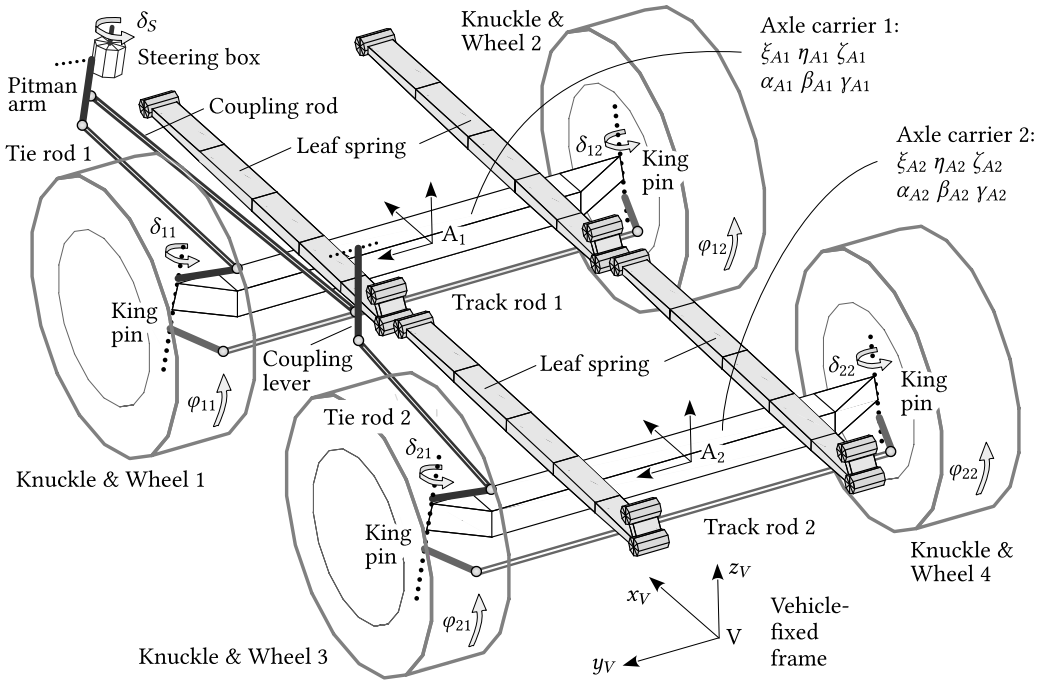

Figure 1 – General layout of dual truck front axles with leaf springs suspension and steering linkage.

to the axle carrier 2. The track rods 1 and 2 couple the knuckle rotations on the left and right side of each axle. The corresponding constraint equations can be solved analytically and provide at each axle ($i = 1, 2$) the knuckle rotations on the right side $\delta_{i2} = \delta_{i2}(\delta_{i1})$ as functions of the knuckle rotations on the left side. Thus, leaving just one degree of freedom for the steer motion (left knuckle rotations relative to the axle carrier) at each axle.

Each of the subsystems front axle 1 and front axle 2 has $6 + 1 = 7$ degrees of freedom then. In case a simplified kinematical suspension model, each axle carrier just performs two unconstrained motions, usually characterized by hub and roll. Then, each subsystem front axle has just $2 + 1 = 3$ degrees of freedom.

Vehicle Equations of Motion and Numerical Solution

The equations of motion for vehicle models, like the virtual test truck or the the virtual test car, described in Rill et al. (2021) and Rill (2022), result in a set of nonlinear first order differential differential equations

$$\dot{y} = K(y)\, z \tag{1}$$

$$M(y)\, \dot{z} = q(y, z, s, u) \tag{2}$$

$$\dot{s} = f(y, z, s, u) \tag{3}$$

The vector y collects the generalized coordinates of the vehicle and the kinematic matrix K defines non-trivial generalized speeds which are arranged in the vector z. The principle of virtual power or Jourdain's principle, respectively, delivers the elements of the mass matrix M and the components of the vector q which summarizes the generalized forces and torques applied to the bodies of the multibody system. The forces and torques may depend on external control inputs collected in the vector u and on additional states s that are required to describe the dynamics of sophisticated force elements, like coupled air springs or tires. The partly implicit Euler-Step

$$y^{k+1} - y^k = h\, K(y^k)\, z^{k+1} \tag{4}$$

$$M(y^k)\left(z^{k+1} - z^k\right) = h\, q\left(y^{k+1}, z^{k+1}, s^{k+1}, u^{k+1}\right) \tag{5}$$

$$s^{k+1} - s^k = h\, f\left(y^k, z^k, s^{k+1}, u^{k+1}\right) \tag{6}$$

is tailored to vehicle dynamics, because it assumes that the dynamics of the force elements, described by the states s, is considerably faster than the dynamics of the vehicle represented by the vectors of generalizes coordinates y and generalized speeds z. The superscripts k and $k+1$ abbreviate the states at time t and $t+h$ where h denotes the integration step size. The control inputs depend on the time t and deliver $u^{k+1} = u(t+h)$ straightforwardly. The truncated Taylor expansion $f^{k+1} \approx f^k + (\partial f / \partial s)\,(s^{k+1} - s^k)$ approximates the function f as defined in (6) and results into

$$\left[I - h\,\frac{\partial f}{\partial s}\right]\left(s^{k+1} - s^k\right) = h\, f\left(y^k, z^k, s^k, u(t+h)\right) \tag{7}$$

where I denotes the matrix of identity with the same dimension as the matrix of partial derivatives $\partial f/\partial s$. The vector of generalized forces and torques required in (5) is approximated by

$$q\left(y^{k+1}, z^{k+1}, s^{k+1}, u^{k+1}\right) \approx q\left(y^k+hK(y^k)z_k, z^k, s^{k+1}, u^{k+1}\right) + \frac{\partial q}{\partial y}\left(y^{k+1} - \left(y^k+hK(y^k)z^k\right)\right) + \frac{\partial q}{\partial z}\left(z^{k+1} - z^k\right) \quad (8)$$

where $y^k+hK(y^k)z_k$ represents an explicit Euler step applied to (1) which enhances the accuracy of the approximation (8) in particular for strongly nonlinear force elements. Then, the Euler step (5) results in

$$\left[M(y^k) - h\left(\frac{\partial q}{\partial z} + h\,\frac{\partial q}{\partial y}\,K(y^k)\right)\right]\left(z^{k+1} - z^k\right) = h\,q\left(y^k+hK(y^k)z_k, z^k, s^{k+1}, u^{k+1}\right) \quad (9)$$

where (4) was used in addition. As demonstrated in Rill (2006b) the contribution of standard force elements, like springs and dampers, to the partial derivatives $\partial q/\partial y$ and $\partial q/\partial z$ is a straight forward task and requires only a small amount of additional computation effort.

The cascade of partly implicit Euler steps, defined by (7), (5), and (4), provides an extremely fast and robust solver tailored to vehicle dynamics. When operated with the standard step size of $h=1$ ms it grants simulation results of sufficient accuracy and when coded in a higher programming language like ANSI C90 it achieves real-time performance for rather complex vehicle models even on small personal computers (Rill et al. 2021).

STEERING SYSTEM MODEL

Model Structure

The steering system model shown in Fig. 2 takes the rotational compliance of the steering column c_S, the stiffness of the tie rods c_1, c_2, and the stiffness of the coupling rod c_C into account. The angles δ_W and δ_S describe the rotations of the steering wheel and the steering box input. The rotation angles of the pitman arm and the coupling lever are limited by stops to the ranges $\delta_P^{min} \le \delta_P \le \delta_P^{max}$ and $\delta_L^{min} \le \delta_L \le \delta_L^{max}$, respectively. The unit vectors e_P and e_L define the rotation axes of the pitman arm and the coupling lever. The former is fixed at point H_1 to the steering box and the latter at point H_2 to the truck frame. The tie rod 1 is attached at joint I_1 to the pitman arm and at joint J_1 to the left knuckle of axle 1. The ends of the coupling rod C_1 and C_2 are connected to the pitman arm and to the coupling lever. The tie rod 2 is attached at joint I_2 to the coupling lever and at joint J_2 to the left knuckle of axle 2.

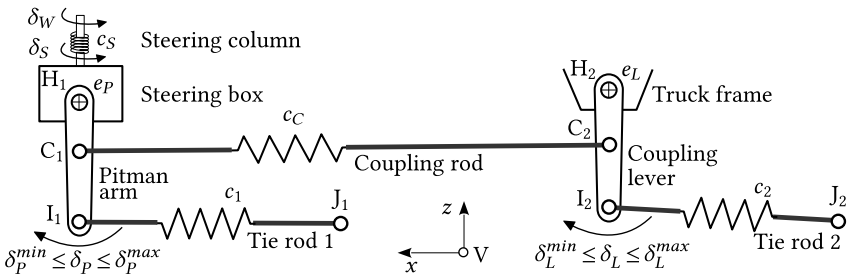

Figure 2 – Steering system for dual steered front axles with modeled compliances.

The design position of the attachment points I_1, J_1, I_2, J_2, and C_1, C_2 deliver the lengths ℓ_{10}, ℓ_{20}, and ℓ_{C0} of the undeformed rods. The actual lengths are given by

$$\ell_1 = \sqrt{r_{I1J1,V}^T\, r_{I1J1,V}}\,; \quad \ell_C = \sqrt{r_{C1C2,V}^T\, r_{C1C2,V}}\,; \quad \ell_2 = \sqrt{r_{I2J2,V}^T\, r_{I2J2,V}} \quad (10)$$

The comma separated index V indicates that the vectors

$$r_{I1J1,V} = r_{VJ1,V} - r_{VI1,V}\,; \quad r_{C1C2,V} = r_{VC2,V} - r_{VC1,V}\,; \quad r_{I2J2,V} = r_{VJ2,V} - r_{VI2,V} \quad (11)$$

pointing from one end of each rod to the other are expressed in the vehicle-fixed reference frame V. The compliance of the rods are modeled by simple linear springs. Then, the forces acting in the tie rod 1, the coupling rod, and in tie rod 2 are provided by

$$F_1 = c_1\,(\ell_1 - \ell_{10}) = c_1\,u_1\,; \quad F_C = c_C\,(\ell_C - \ell_{C0}) = c_C\,u_C\,; \quad F_2 = c_2\,(\ell_2 - \ell_{20}) = c_2\,u_2 \quad (12)$$

where c_1, c_C, c_2 denote the stiffness properties and u_1, u_C, u_2 define the deformations of the corresponding rods.

The tie rods 1 and 2 are attached at J_1 and J_2 to the left wheel bodies of the two axles. Their actual positions with respect to the vehicle fixed reference frame V depend on the generalized coordinates y_{A1} and y_{A2} describing the axle

motions and the rotations of the left wheel bodies about the king pins

$$r_{VJ1,V} = r_{VJ1,V}(y_{A1}) \quad \text{and} \quad r_{VJ2,V} = r_{VJ2,V}(y_{A2}) \tag{13}$$

The momentary positions where the tie rod 1 and the coupling rod are attached to the pitman arm are defined by

$$r_{VI1,V} = r_{VH1,D} + \underbrace{A_P(\delta_P)\, r_{H1I1,D}}_{r_{H1I1,V}} \quad \text{and} \quad r_{VC1,V} = r_{VH1,D} + \underbrace{A_P(\delta_P)\, r_{H1C1,D}}_{r_{H1C1,V}} \tag{14}$$

The matrix $A_P = A_P(\delta_P)$ describes the rotation of the pitman arm about an axis defined by the unit vector $e_{P,V}$. and the vectors $r_{VH1,D}$, $r_{H1I1,D}$, and $r_{H1C1,D}$ characterize the design position of H_1 and the positions of I_1 and C_1 relative to H_1. The momentary positions where the coupling rod and the tie rod 2 are attached to the coupling lever are provided by

$$r_{VC2,V} = r_{VH2,D} + \underbrace{A_L(\delta_L)\, r_{H2C2,D}}_{r_{H2C2,V}} \quad \text{and} \quad r_{VI2,V} = r_{VH2,D} + \underbrace{A_L(\delta_L)\, r_{H2I2,D}}_{r_{H2I2,V}} \tag{15}$$

The matrix $A_L = A_L(\delta_L)$ describes the rotation of the coupling lever about an axis defined by the unit vector $e_{L,V}$ and the vectors $r_{VH2,D}$, $r_{H2C2,D}$, and $r_{H2I2,D}$ characterize the design position of H_2 and the positions of C_2 and I_2 relative to H_2.

Quasi-static Approach

The rotation of the steering box input shaft δ_S and the rotation angle of the coupling lever δ_L are computed in a quasi-static approach. The torsional compliance of the steering column generates the steering torque acting at the steer box input as

$$T_S = c_S\ (\delta_W - \delta_S) = c_S\, \varphi_S \tag{16}$$

where c_S denotes the torsional stiffness of the steering column, $\delta_W = \delta_W(t)$ describes the rotation of the steering wheel and φ_S the torsion angle of the steering column. The principle of virtual work for the steering box and the coupling lever results in

$$\delta\varphi_S\, T_S(\varphi_S) + \delta u_1\, F_1(u_1) + \delta u_C\, F_C(u_C) + \delta u_2\, F_2(u_2) + T_{PL}(\delta_P)\,\delta\delta_P + T_{LL}(\delta_L)\,\delta\delta_L\ = 0 \tag{17}$$

The torques $T_{PL} = T_{PL}(\delta_P)$ and $T_{LL} = T_{LL}(\delta_L)$ model the impact of stops which limit the rotations of the pitman arm and the coupling lever. The transmission of the steering box delivers the momentary and the virtual rotations of the pitman arm as

$$\delta_P = \delta_P(\delta_S) \quad \text{and} \quad \delta\delta_P == \frac{\partial\delta_P}{\partial\varphi_S}\,\delta\varphi_S = \frac{\partial\delta_P}{\partial\delta_S}\,\frac{\partial\delta_S}{\partial\varphi_S}\,\delta\varphi_S = \frac{\partial\delta_P}{\partial\delta_S}\,(-1)\,\delta\varphi_S = -i_S\,\delta\varphi_S \tag{18}$$

The definition of the torsion angle $\varphi_S = \delta_W - \delta_S$ as specified in (16) simply results in $\partial\delta_S/\partial\varphi_S = -1$ and $i_S = \partial\delta_P/\partial\delta_S$ defines the ratio of the steering box which might depend nonlinearly on the rotation of steering box input shaft. Inspecting Equations (12) to (15) the virtual deformations of the rods result in

$$\delta u_1 = \frac{\partial\ell_1}{\partial\delta_P}\,\frac{\partial\delta_P}{\partial\varphi_S}\,\delta\varphi_S \quad \text{with} \quad \frac{\partial\ell_1}{\partial\delta_P} = \frac{r_{I1J1,V}^T}{\ell_1}\,\frac{\partial r_{I1J1,V}}{\partial\delta_P} = e_{I1J1,V}^T\,\frac{\partial r_{I1J1,V}}{\partial\delta_P} \tag{19}$$

$$\delta u_C = \frac{\partial\ell_C}{\partial\delta_P}\,\frac{\partial\delta_P}{\partial\varphi_S}\,\delta\varphi_S + \frac{\partial\ell_C}{\partial\delta_L}\,\delta\delta_L \quad \text{with} \quad \frac{\partial\ell_C}{\partial\delta_{P,L}} = \frac{r_{C1C2,V}^T}{\ell_C}\,\frac{\partial r_{C1C2,V}}{\partial\delta_{P,L}} = e_{C1C2,V}^T\,\frac{\partial r_{C1C2,V}}{\partial\delta_{P,L}} \tag{20}$$

$$\delta u_2 = \frac{\partial\ell_2}{\partial\delta_L}\,\delta\delta_L \quad \text{with} \quad \frac{\partial\ell_2}{\partial\delta_L} = \frac{r_{I2J2,V}^T}{\ell_2}\,\frac{\partial r_{I2J2,V}}{\partial\delta_L} = e_{I2J2,V}^T\,\frac{\partial r_{I2J2,V}}{\partial\delta_L} \tag{21}$$

The pitman arm and the coupling lever perform rotations about axes defined by the unit vectors e_P and e_L and change the momentary positions of the attachment points I_1, C_1 and C_2, I_2, respectively. The partial derivatives of the position vectors defined in (11) are then provided by

$$\frac{\partial r_{I1J1,V}}{\partial\delta_P} = -\frac{\partial r_{VI1,V}}{\partial\delta_P} = -\frac{\partial r_{H1I1,V}}{\partial\delta_P} = -e_{P,V}\times r_{H1I1,V} \tag{22}$$

$$\frac{\partial r_{C1C2,V}}{\partial\delta_P} = -\frac{\partial r_{VC1,V}}{\partial\delta_P} = -\frac{\partial r_{H1C1,V}}{\partial\delta_P} = -e_{P,V}\times r_{H1C1,V} \tag{23}$$

$$\frac{\partial r_{C1C2,V}}{\partial\delta_L} = \frac{\partial r_{VC2,V}}{\partial\delta_L} = \frac{\partial r_{H2C2,V}}{\partial\delta_L} = e_{L,V}\times r_{H2C2,V} \tag{24}$$

$$\frac{\partial r_{I2J2,V}}{\partial\delta_L} = -\frac{\partial r_{VI2,V}}{\partial\delta_L} = -\frac{\partial r_{H2I2,V}}{\partial\delta_L} = -e_{L,V}\times r_{H2I2,V} \tag{25}$$

Inserting Equations (18) to (25) into Equation (17) results in

$$\begin{aligned}\delta\varphi_S\, c_S\,\varphi_S - i_S\,\delta\varphi_S\,\{e_{I1J1,V}^T\,(-e_{P,V}\times r_{H1I1,V})\,F_1 + e_{C1C2,V}^T\,(-e_{P,V}\times r_{H1C1,V})\,F_C\} + \\ \delta\delta_L\,\{e_{C1C2,V}^T\,(e_{L,V}\times r_{H2C2,V})\ F_C + e_{I2J2,V}^T\,(-e_{L,V}\times r_{H2I2,V})\,F_2\} = 0\end{aligned} \tag{26}$$

Virtual displacements and rotations, like $\delta\varphi_S$ and $\delta\delta_L$ are infinite small but do not vanish permanently. Hence, the virtual work (26) delivers two relations

$$T_1 = c_S\varphi_S + i_S e_{P,V}^T\left(r_{H1I1,V}\times e_{I1J1,V}F_1 + r_{H1C1,V}\times e_{C1C2,V}F_C\right) + i_S T_{PL} = 0 \tag{27}$$

$$T_2 = e_{L,V}^T\left(r_{H2I2,V}\times e_{I2J2,V}F_2 - r_{H2C2,V}\times e_{C1C2,V}F_C\right) + T_{LL} = 0 \tag{28}$$

where the property $a^T(b\times c) = b^T(c\times a)$ of a scalar triple product was used to rearrange the equations in the form of torque balances at the steering box and the coupling lever. Introducing the shortcuts

$$a_{11} = e_{P,V}^T r_{H1I1,V}\times e_{I1J1,V} \qquad a_{1C} = e_{P,V}^T r_{H1C1,V}\times e_{C1C2,V} \tag{29}$$

$$a_{22} = e_{L,V}^T r_{H2I2,V}\times e_{I2J2,V} \qquad a_{2C} = e_{L,V}^T r_{H2C2,V}\times e_{C1C2,V} \tag{30}$$

the torque balances simply read as

$$T_1 = c_S\varphi_S + i_S\left(a_{11}F_1 + a_{1C}F_C + T_{PL}\right) = 0 \tag{31}$$

$$T_2 = a_{22}F_2 - a_{2C}F_C + T_{LL} = 0 \tag{32}$$

Numerical Solution

The torque balances represent a set of two nonlinear equations which can be solved iteratively by the Newton-Raphson scheme

$$T(y_S^i) + \frac{\partial T}{\partial y_S}\left(y_S^{i+1}) - y_S^i)\right) = 0 \quad \text{or} \quad y_S^{i+1}) = y_S^i - \left[\frac{\partial T}{\partial y_S}\right]^{-1} T(y_S^i) \quad i = 0, 1, \ldots \tag{33}$$

The torsion angle of the steering column φ_S and the rotation of the coupling lever δ_L as well as the torques T_1 and T_2 are hereby collected in 2×1-vectors

$$y_S = \begin{bmatrix}\varphi_S\\ \delta_L\end{bmatrix}, \quad T(y_S) = \begin{bmatrix}T_1(\varphi_S^i, \delta_L^i)\\ T_2(\varphi_S^i, \delta_L^i)\end{bmatrix}, \quad \text{and} \quad \frac{\partial T}{\partial y_S} = \begin{bmatrix}\frac{\partial T_1}{\partial\varphi_S} & \frac{\partial T_1}{\partial\delta_L}\\ \frac{\partial T_2}{\partial\varphi_S} & \frac{\partial T_2}{\partial\delta_L}\end{bmatrix} \tag{34}$$

which, as a consequence, define the elements of the 2×2-matrix $\partial T/\partial y_S$ of partial torque derivatives. In general, the rotations of the pitman arm δ_P and the coupling lever δ_L will not differ significantly. Then

$$\varphi_S^0 = 0 \quad \text{and} \quad \delta_L^0 = \delta_P(\delta_W) \tag{35}$$

provide appropriate values to start the iteration. The derivatives of the torques $T_1(\varphi_S^i, \delta_L^i)$ and $T_2(\varphi_S^i, \delta_L^i)$ as defined in (27) and (28) result in

$$\begin{aligned}\frac{\partial T_1}{\partial\varphi_S} = c_S + i_S e_{P,V}^T\Bigg(&\frac{\partial r_{H1I1,V}}{\partial\delta_P}\times e_{I1J1,V}F_1 + r_{H1I1,V}\times e_{I1J1,V}\frac{\partial F_1}{\delta_P}\\ &+ \frac{\partial r_{H1C1,V}}{\partial\delta_P}\times e_{C1C2,V}F_C + r_{H1C1,V}\times e_{C1C2,V}\frac{\partial F_C}{\partial\delta_P}\Bigg)(-i_S)\\ &+ i_S\frac{\partial T_{PL}}{\partial\delta_P}i_S(-1)\end{aligned} \tag{36}$$

$$\frac{\partial T_1}{\partial\delta_L} = i_S e_{P,V}^T r_{H1C1,V}\times e_{C1C2,V}\frac{\partial F_C}{\partial\delta_L} \tag{37}$$

$$\frac{\partial T_2}{\partial\varphi_S} = -e_{L,V}^T r_{H2C2,V}\times e_{C1C2,V}\frac{\partial F_C}{\partial\delta_P}(-i_S) \tag{38}$$

$$\begin{aligned}\frac{\partial T_2}{\partial\delta_L} = e_{L,V}^T\Bigg(&\frac{\partial r_{H2I2,V}}{\partial\delta_L}\times e_{I2J2,V}F_2 + r_{H2I2,V}\times e_{I2J2,V}\frac{\partial F_2}{\partial\delta_L}\\ &- \frac{\partial r_{H2C2,V}}{\partial\delta_L}\times e_{C1C2,V}F_C - r_{H2C2,V}\times e_{C1C2,V}\frac{\partial F_C}{\partial\delta_L}\Bigg) + \frac{\partial T_{LL}}{\partial\delta_L}\end{aligned} \tag{39}$$

The partial derivatives of the position vectors are already computed in (22) to (25). The force derivatives result in

$$\begin{aligned}\frac{\partial F_1}{\partial\delta_P} &= c_1\frac{\partial\ell_1}{\partial\delta_P} = c_1 e_{I1J1}^T\frac{\partial r_{I1J1}}{\partial\delta_P} = c_1 e_{I1J1}^T(-e_P\times r_{H1I1}) = -c_1 e_P^T(r_{H1I1}\times e_{I1J1}) = -c_1 a_{11}\\ \frac{\partial F_C}{\partial\delta_L} &= c_C\frac{\partial\ell_C}{\partial\delta_L} = c_C e_{C1C2}^T\frac{\partial r_{C1C2}}{\partial\delta_L} = c_C e_{C1C2}^T(e_L\times r_{H2C2}) = c_C e_L^T(r_{H2C2}\times e_{C1C2}) = c_C a_{2C}\\ \frac{\partial F_C}{\partial\delta_P} &= c_C\frac{\partial\ell_C}{\partial\delta_P} = c_C e_{C1C2}^T\frac{\partial r_{C1C2}}{\partial\delta_P} = c_C e_{C1C2}^T(-e_P\times r_{H1C1}) = -c_C e_P^T(r_{H1C1}\times e_{C1C2}) = -c_C a_{1C}\\ \frac{\partial F_2}{\partial\delta_L} &= c_2\frac{\partial\ell_2}{\partial\delta_L} = c_2 e_{I2J2}^T\frac{\partial r_{I2J2}}{\partial\delta_L} = c_2 e_{I2J2}^T(-e_L\times r_{H2I2}) = -c_2 e_L^T(r_{H2I2}\times e_{I2J2}) = c_2 a_{22}\end{aligned} \tag{40}$$

where all comma separated subscripts V, indicating that the corresponding vector is expressed in the frame-fixed coordinate system, are omitted for the sake of simplicity. The final results incorporate the partial derivatives $\partial\varphi_P/\partial\varphi_S$, $\partial\ell_1/\partial\varphi_S$, $\partial\ell_C/\partial\varphi_S$, $\partial\ell_C/\partial\delta_L$, and $\partial\ell_2/\partial\delta_L$ defined in (18) and (19) to (21) as well as the abbreviations (29) and (30).

The analytical computation of the elements of the matrix of partial torque derivatives $\partial T/\partial y_S$ makes the Newton algorithm (33) converge very fast and robust even with the rather simple starting values as provided by (35). The partial derivatives provided in this section and in particular the inverse of the 2×2-matrix $\partial T/\partial y_S$ also deliver the effective stiffness properties of the tie rods which are required for an implicit integration step.

Effective Stiffness Properties

The tie rod forces F_1 and F_2 as defined by (10) to (12) depend on the position vectors $r_{VJ1,V}$ and $r_{VJ2,V}$ which describe the momentary positions of the axle-fixed joints J_1 and J_2. As a consequence, the torsional angle of the steering column φ_S and the rotation angle of the coupling lever δ_L computed via the torque balances (31) and (32) also depend on $r_{VJ1,V}$ and $r_{VJ2,V}$. Then, the total derivatives of the vectorized torque balance T with respect to $r_{VJ1,V}$ and $r_{VJ2,V}$ result in

$$\left(\frac{\partial T}{\partial r_{VJ1,V}}\right)_{tl} = \frac{\partial T}{\partial r_{VJ1,V}} + \frac{\partial T}{\partial y_S}\frac{\partial y_S}{\partial r_{VJ1,V}} = 0 \quad \text{and} \quad \left(\frac{\partial T}{\partial r_{VJ2,V}}\right)_{tl} = \frac{\partial T}{\partial r_{VJ2,V}} + \frac{\partial T}{\partial y_S}\frac{\partial y_S}{\partial r_{VJ2,V}} = 0 \tag{41}$$

and deliver the derivatives of the vector y_S with respect to the position vectors $r_{VJ1,V}$ and $r_{VJ2,V}$. The partial derivatives of the torque vector T with respect to the position vectors $r_{VJ1,V}$ and $r_{VJ2,V}$ result in

$$\frac{\partial T}{\partial r_{VJ1,V}} = \begin{bmatrix} \dfrac{\partial T_1}{\partial r_{VJ1,V}} \\ \dfrac{\partial T_2}{\partial r_{VJ1,V}} \end{bmatrix} = \begin{bmatrix} i_S\, a_{11}\dfrac{\partial F_1}{\partial r_{VJ1,V}} \\ 0 \end{bmatrix} \quad \text{and} \quad \frac{\partial T}{\partial r_{VJ2,V}} = \begin{bmatrix} \dfrac{\partial T_1}{\partial r_{VJ1,V}} \\ \dfrac{\partial T_2}{\partial r_{VJ1,V}} \end{bmatrix} = \begin{bmatrix} 0 \\ a_{22}\dfrac{\partial F_2}{\partial r_{VJ2,V}} \end{bmatrix} \tag{42}$$

where

$$\frac{\partial F_1}{\partial r_{VJ1,V}} = c_1\, e_{I1J1,V}^T \frac{\partial r_{I1J1,V}}{\partial r_{VJ1,V}} = c_1\, e_{I1J1,V}^T \frac{\partial r_{VJ1,V}}{\partial r_{VJ1,V}} = c_1\, e_{I1J1,V}^T \tag{43}$$

$$\frac{\partial F_2}{\partial r_{VJ2,V}} = c_2\, e_{I2J2,V}^T \frac{\partial r_{I2J2,V}}{\partial r_{VJ2,V}} = c_2\, e_{I2J2,V}^T \frac{\partial r_{VJ2,V}}{\partial r_{VJ2,V}} = c_2\, e_{I2J2,V}^T \tag{44}$$

provides the partial derivatives of the tie rod forces F_1 and F_2 with respect to the position vectors $r_{VJ1,V}$ and $r_{VJ2,V}$. The partial derivative of the torque vector T with respect to the vector y_S is defined in (33) and (36) to (39) provide it element by element. Then, the total torque derivatives (41) deliver

$$\frac{\partial y_S}{\partial r_{VJ1,V}} = -\left[\frac{\partial T}{\partial y_S}\right]^{-1}\left(\frac{\partial T}{\partial r_{VJ1,V}}\right)_{tl} = -\left[\frac{\partial T}{\partial y_S}\right]^{-1}\begin{bmatrix} i_S\, a_{11}\dfrac{\partial F_1}{\partial r_{VJ1,V}} \\ 0 \end{bmatrix} = -\left[\frac{\partial T}{\partial y_S}\right]^{-1}\begin{bmatrix} i_S\, a_{11}\, c_1\, e_{I1J1,V}^T \\ 0 \end{bmatrix} \tag{45}$$

$$\frac{\partial y_S}{\partial r_{VJ2,V}} = -\left[\frac{\partial T}{\partial y_S}\right]^{-1}\left(\frac{\partial T}{\partial r_{VJ2,V}}\right)_{tl} = -\left[\frac{\partial T}{\partial y_S}\right]^{-1}\begin{bmatrix} 0 \\ a_{22}\dfrac{\partial F_2}{\partial r_{VJ2,V}} \end{bmatrix} = -\left[\frac{\partial T}{\partial y_S}\right]^{-1}\begin{bmatrix} 0 \\ a_{22}\, c_2\, e_{I2J2,V}^T \end{bmatrix} \tag{46}$$

where the 2×2-matrix of partial torque derivatives $\partial T/\partial y_S$ is defined in (34) and its inverse is already used in (33). The total changes of the tie rod forces F_1 and F_2 with respect to the position vectors $r_{VJ1,V}$ and $r_{VJ2,V}$ are defined by

$$\begin{aligned}
\left(\frac{\partial F_1}{\partial r_{VJ1,V}}\right)_{tl} &= \frac{\partial F_1}{\partial r_{VJ1,V}} + \frac{\partial F_1}{\partial y_S}\frac{\partial y_S}{\partial r_{VJ1,V}} \\
&= c_1\, e_{I1J1,V}^T + \begin{bmatrix} \dfrac{\partial F_1}{\partial\delta_P}\dfrac{\partial\delta_P}{\partial\varphi_S} & \dfrac{\partial F_1}{\partial\delta_L} \end{bmatrix}\left(-\left[\frac{\partial T}{\partial y_S}\right]^{-1}\begin{bmatrix} i_S\, a_{11}\, c_1\, e_{I1J1,V}^T \\ 0 \end{bmatrix}\right) \\
&= c_1\, e_{I1J1,V}^T - \begin{bmatrix} -c_1\, a_{11}\,(-i_S) & 0 \end{bmatrix}\left[\frac{\partial T}{\partial y_S}\right]^{-1}\begin{bmatrix} i_S\, a_{11}\, c_1 \\ 0 \end{bmatrix} e_{I1J1,V}^T \\
&= c_1\left(1 - \begin{bmatrix} 1 & 0 \end{bmatrix}\left[\frac{\partial T}{\partial y_S}\right]^{-1}\begin{bmatrix} 1 \\ 0 \end{bmatrix} c_1\,(i_S\, a_{11})^2\right) e_{I1J1,V}^T = c_{11}^q\, e_{I1J1,V}^T
\end{aligned} \tag{47}$$

$$\begin{aligned}
\left(\frac{\partial F_2}{\partial r_{VJ1,V}}\right)_{tl} &= \frac{\partial F_2}{\partial r_{VJ1,V}} + \frac{\partial F_2}{\partial y_S}\frac{\partial y_S}{\partial r_{VJ1,V}} \\
&= 0 + \begin{bmatrix} \dfrac{\partial F_2}{\partial\delta_P}\dfrac{\partial\delta_P}{\partial\varphi_S} & \dfrac{\partial F_2}{\partial\delta_L} \end{bmatrix}\left(-\left[\frac{\partial T}{\partial y_S}\right]^{-1}\begin{bmatrix} i_S\, a_{11}\, c_1\, e_{I1J1,V}^T \\ 0 \end{bmatrix}\right) \\
&= -i_S\begin{bmatrix} 0 & c_2\, a_{22} \end{bmatrix}\left[\frac{\partial T}{\partial y_S}\right]^{-1}\begin{bmatrix} c_1\, a_{11} \\ 0 \end{bmatrix} e_{I1J1,V}^T = c_{21}^q\, e_{I1J11,V}^T
\end{aligned} \tag{48}$$

$$
\begin{aligned}
\left(\frac{\partial F_1}{\partial r_{VJ2,V}}\right)_{tl} &= \frac{\partial F_1}{\partial r_{VJ2,V}} + \frac{\partial F_1}{\partial y_S}\frac{\partial y_S}{\partial r_{VJ2,V}} \\
&= 0 + \begin{bmatrix} \frac{\partial F_1}{\partial \delta_P}\frac{\partial \delta_P}{\partial \varphi_S} & \frac{\partial F_1}{\partial \delta_L} \end{bmatrix} \left(-\left[\frac{\partial T}{\partial y_S}\right]^{-1} \begin{bmatrix} 0 \\ a_{22}\, c_2\, e_{I2J2,V}^T \end{bmatrix} \right) \\
&= -i_S \begin{bmatrix} c_1\, a_{11} & 0 \end{bmatrix} \left[\frac{\partial T}{\partial y_S}\right]^{-1} \begin{bmatrix} 0 \\ a_{22}\, c_2 \end{bmatrix} e_{I2J2,V}^T = c_{12}^q\, e_{I2J12,V}^T \\
\left(\frac{\partial F_2}{\partial r_{VJ2,V}}\right)_{tl} &= \frac{\partial F_2}{\partial r_{VJ2,V}} + \frac{\partial F_2}{\partial y_S}\frac{\partial y_S}{\partial r_{VJ2,V}} \\
&= c_2\, e_{I2J2,V}^T + \begin{bmatrix} \frac{\partial F_2}{\partial \delta_P}\frac{\partial \delta_P}{\partial \varphi_S} & \frac{\partial F_2}{\partial \delta_L} \end{bmatrix} \left(-\left[\frac{\partial T}{\partial y_S}\right]^{-1} \begin{bmatrix} 0 \\ a_{22}\, c_2\, e_{I2J2,V}^T \end{bmatrix} \right) \\
&= c_2\, e_{I2J2,V}^T - \begin{bmatrix} 0 & c_2\, a_{22} \end{bmatrix} \left[\frac{\partial T}{\partial y_S}\right]^{-1} \begin{bmatrix} 0 \\ a_{22}\, c_2 \end{bmatrix} e_{I2J2,V}^T \\
&= c_2 \left(1 - \begin{bmatrix} 0 & 1 \end{bmatrix} \left[\frac{\partial T}{\partial y_S}\right]^{-1} \begin{bmatrix} 0 \\ 1 \end{bmatrix} c_2\, a_{22}^2 \right) e_{I2J12,V}^T = c_{22}^q\, e_{I2J12,V}^T
\end{aligned}
\tag{49, 50}
$$

Where c_{11}^q, c_{22}^q, and $c_{12}^q = c_{21}^q$ represent the effective stiffness properties of the tie rods and the corresponding coupling term.

Generalized Forces and Derivatives

The differential equation (2) defining the dynamics of the vehicle is driven by the vector q which collects the generalized forces and torques applied to the multibody model. According to the principle of virtual power the contributions of the tie rod forces F_1 and F_2 are defined as follows

$$
q_{S1} = \left(\frac{\partial v_1}{\partial z_{A1}}\right)^T F_1 \quad \text{and} \quad q_{S2} = \left(\frac{\partial v_2}{\partial z_{A2}}\right)^T F_2 \tag{51}
$$

where $\partial v_1/\partial z_{A1}$ and $\partial v_2/\partial z_{A2}$ denote the partial velocities of the tie rod deformations. Similar to (1) the differential equations

$$
\dot{y}_{A1} = K_{A1}(y_{A1})\, z_{A1} \quad \text{and} \quad \dot{y}_{A2} = K_{A2}(y_{A2})\, z_{A2} \tag{52}
$$

provide the generalized speeds of the axle subsystems z_{A1}, z_{A2} via the kinematic matrices K_{A1}, K_{A2}. The virtual velocities δv_i of the tie rod defirmations $i = 1, 2$ provide the partial velocities of the tie rod deformations as

$$
\delta v_i = \frac{\partial v_i}{\partial z_{Ai}}\, \delta z_{Ai} = \frac{\partial \dot{u}_i}{\partial \dot{y}_{Ai}}\frac{\partial \dot{y}_{Ai}}{\partial z_{Ai}}\, \delta z_{Ai} = \frac{\partial u_i}{\partial y_{Ai}} K_{Ai}\, \delta z_{Ai} \quad \text{or} \quad \frac{\partial v_i}{\partial z_{Ai}} = \frac{\partial u_i}{\partial y_{Ai}} K_{Ai} = \frac{\partial u_i}{\partial r_{VJi,V}}\frac{\partial r_{VJi,V}}{\partial y_{Ai}} K_{Ai} \tag{53}
$$

The subsystems front axle $i = 1$ and front axle $i = 2$ provide the partial derivatives of the position vectors $r_{VJ1,V}$ and $r_{VJ2,V}$ with respect to the generalized axle coordinates y_{A1} and y_{A2} as well as the kinematic matrices K_{A1} and K_{A2}. Similar to (19) and (21) the partial derivatives of the tie rod deformations with respect to the position vectors are simply given by

$$
\frac{\partial u_i}{\partial r_{VJi,V}} = e_{IiJi,V}^T \frac{\partial r_{IiJi,V}}{\partial r_{VJi,V}} = e_{IiJi,V}^T\, (-1) = -e_{IiJi,V}^T \tag{54}
$$

where (11) was processed in addition. Then, the contributions of the tie rod forces (51) read as

$$
q_{S1} = \left(-e_{I1J1,V}^T \frac{\partial r_{VJ1,V}}{\partial y_{A1}} K_{A1} \right)^T F_1 \quad \text{and} \quad q_{S2} = \left(-e_{I2J2,V}^T \frac{\partial r_{VJ2,V}}{\partial y_{A2}} K_{A2} \right)^T F_2 \tag{55}
$$

The partly implicit Euler step (5) requires the derivatives of the generalized force vector q with respect to the vector of generalized coordinates y in the form of the matrix $\partial q/\partial y\, K$, where q and y are the vectors of generalized forces and coordinates and K names the overall kinematic matrix. The steering forces F_1 and F_2 depend on the vectors y_{A1} and y_{A2} which collect the generalized coordinates describing the subsystems front axle 1 and front axle 2. Then, the generalized force vectors q_{S1} and q_{S2} contribute the submatrix

$$
\frac{\partial q_{S1/S2}}{\partial y_{A1/A2}} K_{A1/A2} = \begin{bmatrix} \frac{\partial q_{S1}}{\partial y_{A1}} K_{A1} & \frac{\partial q_{S1}}{\partial y_{A2}} K_{A2} \\ \frac{\partial q_{S2}}{\partial y_{A1}} K_{A1} & \frac{\partial q_{S2}}{\partial y_{A2}} K_{A2} \end{bmatrix} \tag{56}
$$

to the overall matrix of partial derivatives. The concept of non-perfect multibody vehicle models, as applied in Rill et al. (2021) and Rill (2022), considers the change of the partial velocities due to the vector of generalized coordinates or speeds

as comparatively small. Then, the partial derivative of the vector q_{S1} with respect to the vector y_{A1} for example can be approximated by

$$\frac{\partial q_{S1}}{\partial y_{A1}} \approx \left(\frac{\partial v_1}{\partial z_{A1}}\right)^T \frac{\partial F_1}{\partial y_{A1}} = \left(\frac{\partial v_1}{\partial z_{A1}}\right)^T \left(\frac{\partial F_1}{\partial r_{VJ1,V}}\right)_{tl} \frac{\partial r_{VJ1,V}}{\partial y_{A1}} \tag{57}$$

The subsystem front axle 1 provides the partial derivative of the position vector $r_{VJ1,V}$ with respect to the generalized axle coordinates y_{A1} and (47) delivers the total derivative of the tie rod force F_1 with respect to $r_{VJ1,V}$. Then, the parts of the submatrix (56) are defined as follows

$$\frac{\partial q_{Si}}{\partial y_{Aj}} K_{Aj} \approx \left(\frac{\partial v_i}{\partial z_{Aj}}\right)^T \left(\frac{\partial F_i}{\partial r_{VJj,V}}\right)_{tl} \frac{\partial r_{VJj,V}}{\partial y_{Aj}} K_{Aj} = \left(-e_{IiJj,V}^T \frac{\partial r_{VJi,V}}{\partial y_{Aj}} K_{Aj}\right)^T c_{ij}^q e_{IiJj,V}^T \frac{\partial r_{VJi,V}}{\partial y_{Aj}} K_{Aj} \quad \begin{matrix} i=1,2 \\ j=1,2 \end{matrix} \tag{58}$$

where (47) to (50) as well as (53) and (54) are taken into account and the kinematic matrices K_{Aj} for $j = 1,2$ follow from the definition of non-trivial generalized axle speeds in (52). The parts $\partial q_{S1}/\partial y_{A2}$ and $\partial q_{S2}/\partial y_{A1}$ represent the effect of the coupling rod which applies forces to both axle subsystems.

RESULTS

The force based steering system model can easily be integrated into multibody truck models. To avoid overshoots or high-frequent oscillations in the steering system, the tie rod and coupling rod forces, defined in (12) as simple springs, are supplemented by viscous parts which are simply adjusted to the stiffness properties of the rods. The main features of the virtual test truck representing a fully laden 10-wheeler with a total mass of 40 t are provided in Fig. 3.

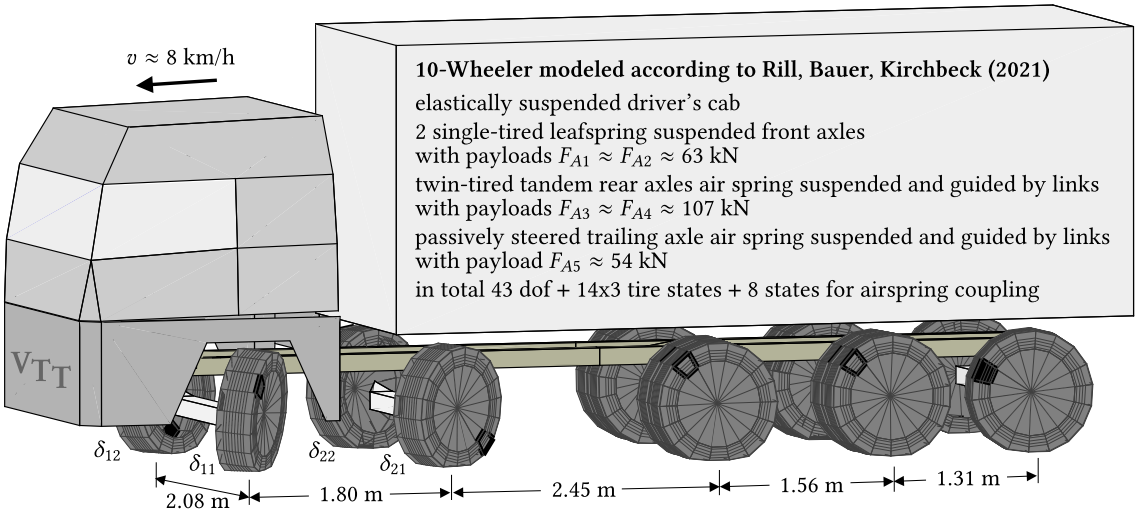

Figure 3 – Main model properties of a 10-wheeler.

At first, the virtual test truck is slowly driven on a flat and horizontal surface. The steering wheel is ramp-like moved to the right and to the left as defined by Tab. 1. The results related to the steering system of the 10-wheeler during

Table 1 – Lookup table providing the steering wheel angle as a function of time.

t in seconds	0.0	5.0	8.0	12.0	18.0	21.0	24.0	25.0
δ_W in degree	0.0	0.0	-720.0	-720.0	+720.0	+720.0	0.0	0.0

tight cornering at low driving velocity are plotted in Fig. 4. It can be seen that the pitman arm rotation $\delta_P(t)$ and the rotation of the coupling lever $\delta_L(t)$ follow the pre-defined steering wheel input $\delta_W(t)$ where the ratio of the steering box can be estimated roughly as $i_S \approx \delta_P^{max}/\delta_W^{max} = 50/720 = 0.07$ by inspecting Tab. 1 and the left plot in Fig. 4. The ramp like steer input results in impulse like tie rod forces. The knuckle rotations δ_{11} to δ_{22} about the king pin axes correspond approximately to the wheel steering angles. Their time histories trace the Ackermann steering geometry by generating larger rotation angles at the inner curve wheels and by reducing the steering angles at the second axle, in general. However, the two twin-tired rigid axles within the tandem rear axle suspension are not steered which makes the Ackermann steering geometry just a rough guess. That is why, the standard layout of a dual front axle suspension simply consists of two identical axles. As a consequence, the time histories of the lateral forces show quite different relations at front axle 1 and 2 between the the left (F_{y11}, F_{y21}) and right tires (F_{y12}, F_{y22}). Even at this extreme steering maneuver, the number of iterations, required to solve the nonlinear torque balances (31) and (32), is limited to a single digit number.

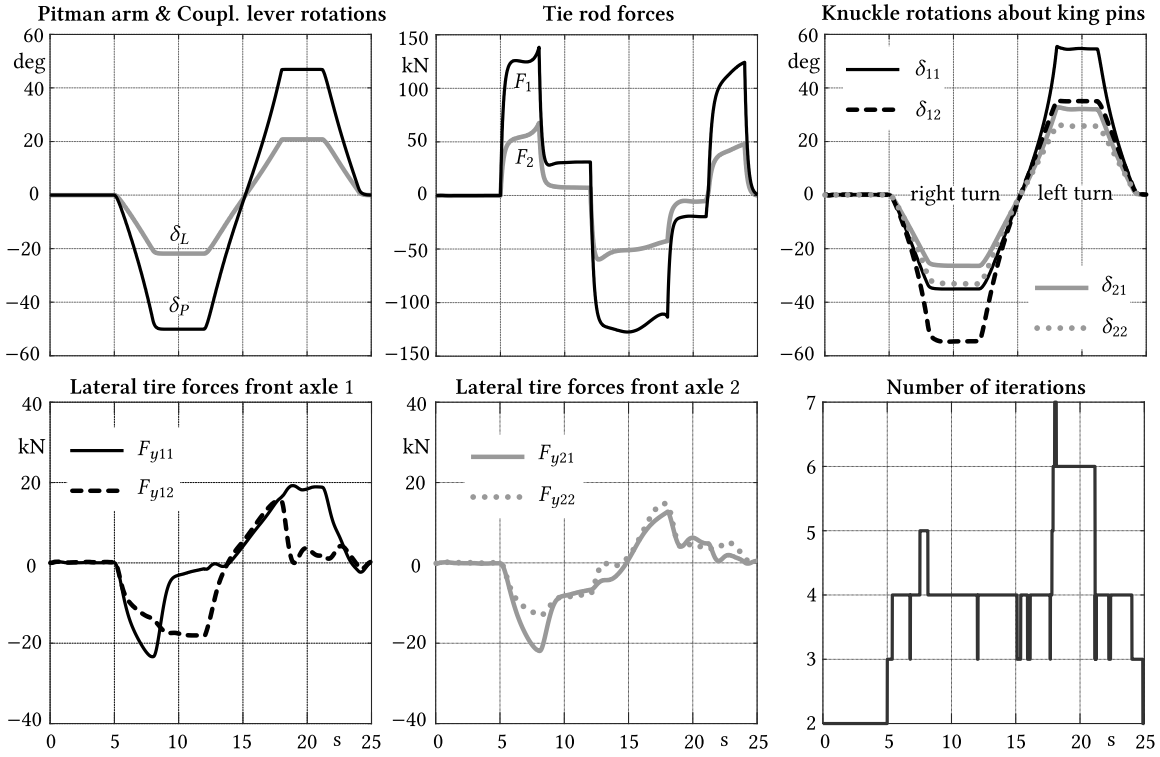

Figure 4 – Steering system related results of a 10-wheeler during tight cornering at low speed.

The virtual test truck models each leaf spring by a 5-link model which reproduces the suspension kinematics very accurately (Rill et al. 2022). In general, the layout of the steering system is adjusted to the kinematics of the front axle suspension system which makes it less sensitive to the impact of axle motions induced by varying wheel loads.

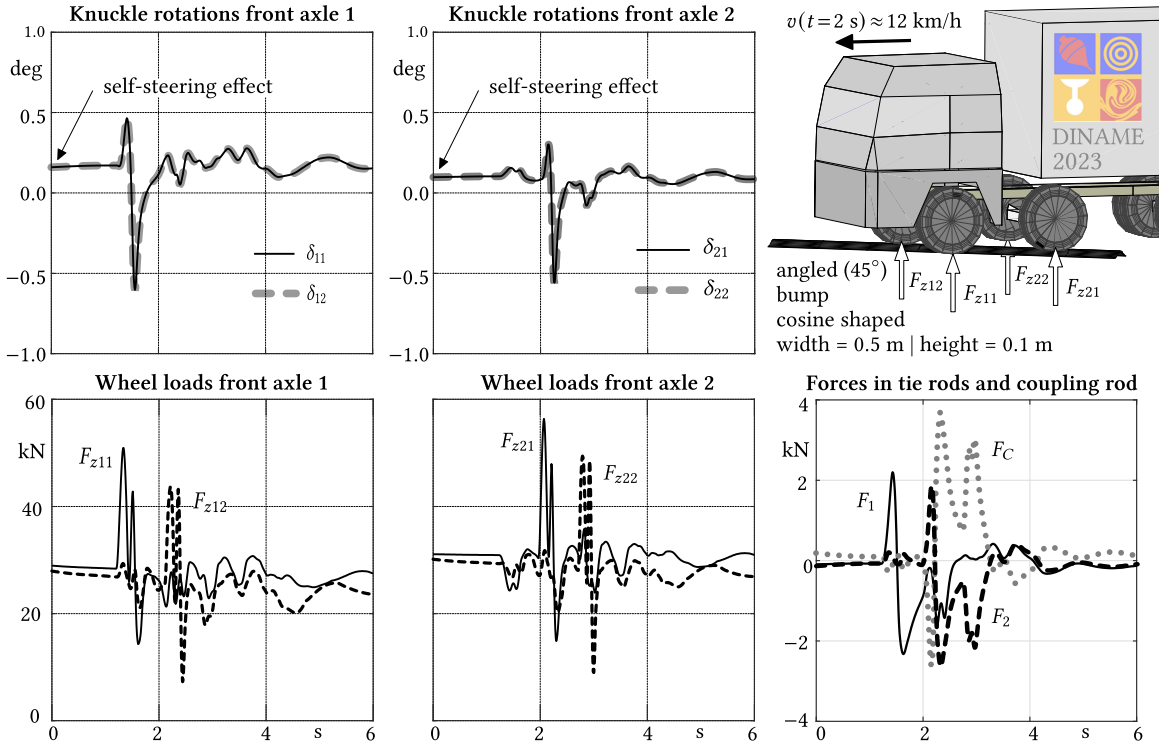

Figure 5 – Wheel steering angles, wheel loads, and steering forces when crossing an angled bump.

Some results of a bump crossing are plotted in Fig. 5. At the beginning ($t = 0$ s) the truck is driving with a velocity of $v(t=0) \approx 5$ km/h. During the bump crossing it is slowly accelerated to $v(t=6\ \mathrm{s}) \approx 25$ km/h. The steering wheel is kept

fixed to $\delta_W = 0°$. The suspension travel at the front axles related to the loading condition of the truck results in a small self-steering effect indicated by the wheel steering angles of $\delta_{11}(t=0) = \delta_{12}(t=0) = 0.16°$ and $\delta_{21}(t=0) = \delta_{22}(t=0) = 0.10°$, respectively. Due to the angled orientation of the bump, the left wheel of the first front axle comes at first into contact with the bump. The time history of the corresponding wheel load $F_{z11}(t)$ in the impact interval of $1.2\ \text{s} \le t \le 1.8\ \text{s}$ shows a double peak on the wheel load increase and a simple peak on the wheel load decrease. The double peak is caused by the compliance of the axle suspension and the steering system. The time histories of the tie rod forces $F_1(t)$ and $F_2(t)$ roughly correspond to the steering movements $\delta_{11}(t) \approx \delta_{12}(t)$ and $\delta_{21}(t) \approx \delta_{22}(t)$ of the wheels at both front axles. In the time interval $2.0\ \text{s} \le t \le 3.5\ \text{s}$ the right wheel at the first and the left wheel of the second front axle hit nearly simultaneously the bump. The impacts on the wheel steering motions counteract itself and cause a distinct reaction in the time history of the coupling rod force $F_C(t)$.

In this standard layout of a dual front axle suspension system the axle hub and roll movements caused by the bump crossing induce only slight steer motions. A standard steering system is also less sensitive to the S-shaped bending modes of the leaf springs occurring at full braking maneuvers (Rill et al. 2022).

SUMMARY

The presented steering system restricts the axle motions just by the tie rod forces and not by kinematical constraints. That is why, it can easily be integrated in multibody truck models. It forms a perfect supplement to comparatively lean, but sufficiently accurate multibody suspension models. The quasi-static solution is sufficiently accurate and fast. It also provides the partial derivatives required for an implicit solver in analytical form. In this particular case, the simulation of the 10-wheeler truck model, as specified in Fig. 3, executed on a Personal Computer with a 2,7 GHz Quad-Core Intel Core i7 was 10-times faster than real-time. The virtual test truck, coded in ANSI-C, incorporates the 5-link model of a leaf spring suspension, the TMeasy tire model, and it solves the set of first order differential equations with a partial implicit solver at a constant step-size of 1 ms.

REFERENCES

Rill, G., 1997, “Vehicle Modeling for Real Time Applications”, Journal of the Brazilian Society of Mechanical Sciences - RBCM XIX.2, pp. 192–206.

Rill, G., 2006a, “Vehicle Modeling by Subsystems”, Journal of the Brazilian Society of Mechanical Sciences & Engineering - ABCM XXVIII.4 pp. 431–443.

Rill, G., 2006b, “A modified implicit Euler Algorithm for solving Vehicle Dynamic Equations” Multibody System Dynamics, Vol. 15, Issue 1, pp. 1–24.

Qin, G., Sun, Y., Yunqing Zhang, Y., and Chen, L., 2012, “Analysis and Optimization of the Double-Axle Steering Mechanism with Dynamic Loads”, The Open Mechanical Engineering Journal, Vol. 6, (Suppl 1-M2) pp. 26–39.

Rill, G., 2013, “TMeasy – The Handling Tire Model for all Driving Situations”, Proceedings of the XV International Symposium on Dynamic Problems of Mechanics (DINAME 2013). Ed. Savi, M., Buzios, RJ, Brazil.

Topaç, M. M., Karaca, M., and Kuleli, B., 2019, “A Design Optimization Study for the Multi-axle Steering System of an 8×8 ARFF Vehicle”, Proceedings of the Applied Physics, System Science and Computers III, Ed. Ntalianis, K et al., pp. 342–347.

Bruni, S., Meijaard, J.P., Rill, G., Schwab A. L., 2020, “State-of-the-art and challenges of railway and road vehicle dynamics with multibody dynamics approaches”, Multibody System Dynamics, Vol 49, pp. 1–32.

Rill, G., Bauer, F., and Kirchbeck, M., 2021, “VTT – a virtual test truck for modern simulation tasks”, Vehicle System Dynamics, Vol. 59, No. 4, pp. 635–656.

Rill, G., Bauer, F., and Topcagic, E., 2022, “Performance of leaf spring suspended axles in model approaches of different complexities”, Vehicle System Dynamics, Vol. 60, No. 8, pp. 2871-2889.

Rill, G., 2022 “A Three-Dimensional and Nonlinear Virtual Test Car”, `https://enoc2020.sciencesconf.org/381007/document`

RESPONSIBILITY NOTICE

The author is the only responsible for the printed material included in this paper.